Fast relative sensor orientation estimation in the presence of real-world disturbances

Remmerswaal, Evan ; Weygers, Ive; Smit, Gerwin; Kok, Manon

DOI
10.23919/ECC54610.2021.9654849

Publication date
2021

Document Version
Final published version

Published in
Proceedings of the European Control Conference (ECC 2021)

2021 European Control Conference (ECC)
June 29 - July 2, 2021. Rotterdam, Netherlands

Fast relative sensor orientation estimation in the presence of real-world disturbances

Evan Remmerswaal[1], Ive Weygers[2], Gerwin Smit[3] and Manon Kok[1]

***Abstract*— We present a novel approach to estimate the relative sensor orientation from inertial sensors placed on connected body segments. Drift in the relative orientation estimates obtained by integrating the gyroscope measurements is corrected solely by incorporating common information in the inertial sensor measurements due to the connection of the body segments. We solve the estimation problem using a complementary filtering implementation to reduce the computational complexity. We study its robustness under common real-world model violations, e.g., soft tissue artifacts and spikes in the acceleration signals due to impacts. The efficacy of the method is illustrated with numerical simulations and is compared to a multiplicative extended Kalman filter implementation, both with and without outlier rejection. In addition, a human experiment strengthened the simulation results under realistic sensor errors.**

I. INTRODUCTION

In recent years, the use of body-attached inertial measurement units (IMUs) for movement analysis applications is receiving increasing interest [1], [2], [3], [4]. Within movement analysis, interest is often in kinematics, which requires estimation of the relative sensor orientation from sensors placed upon the body [5]. Widely used techniques to determine these relative sensor orientations for kinematic analysis are either based on optoelectronics or based on inertial sensors.

In contrast to standard optoelectronic systems, inertial sensor based methods allow for a prolonged kinematic analysis in outside-lab environments over multiple days or even weeks [6]. It is therefore necessary to develop algorithms that are both computationally efficient and that result in accurate orientation estimates in real-world scenarios. Common real-world disturbances include large acceleration signals due to impacts, and soft tissue artifacts (STA). These result in violations of the model assumptions that are commonly used in orientation estimation, such as a rigid connection between skin-attached sensor and segment. In this work, we present a novel algorithm to estimate the relative sensor orientation between two sensors placed on connected body segments as illustrated in Fig. 1. We show that the algorithm is computationally efficient and study its robustness against real-world disturbances.

[1]Evan Remmerswaal and Manon Kok are with the Delft Center for Systems and Control, Delft University of Technology, the Netherlands, j.w.g.remmerswaal@student.tudelft.nl, m.kok-1@tudelft.nl.

[2]Ive Weygers is with the Department of Movement and Rehabilitation Sciences, KU Leuven Campus Bruges, Belgium, ive.weygers@kuleuven.be.

[3]Gerwin Smit is with the Department of BioMechanical Engineering, Delft University of Technology, the Netherlands, g.smit@tudelft.nl.

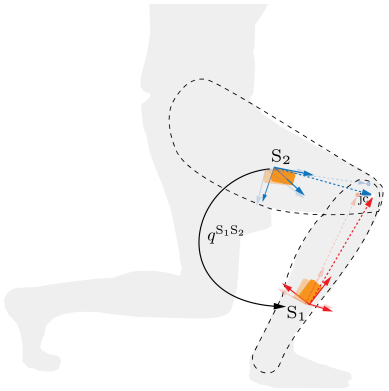

Fig. 1: We estimate the relative orientation $q^{S_1S_2}$ between two IMUs S_1 and S_2 placed on adjacent segments. We assume that measurements from both sensors can be used to correctly approximate the acceleration at the joint center jc and study the effect of violations of this assumption on the quality of the estimates.

Algorithms to estimate the sensor orientation from inertial measurements typically integrate the measurements of the angular velocity, provided by the gyroscope. The resulting orientation estimates are accurate on a short time scale. However, integration of the noisy and biased gyroscope measurements results in an increase of the orientation error over time [7]. Accelerometers are often assumed to predominantly measure gravity and are therefore often used to remove the drift in the inclination part of the orientation estimate. Magnetometers can be used to remove the drift in the heading, assuming that the sensor only measures a constant local magnetic field. Since the magnetic field is typically different at different sensor locations, the use of magnetometers is considered to be problematic when analyzing human motion using multiple body-attached inertial sensors [8], [9].

Recent algorithms to estimate the relative orientation between body segments have therefore focused on magnetometer-free estimation approaches by including kinematic models concerning the joint configurations and their degrees of freedom [10], [11], [12]. For the most general three-dimensional ball-and-socket joint type, we can assume that adjacent segments are connected (which is most often valid, up to small joint translational movements [13]) to define a more specific sensor fusion problem on 'estimating the relative pose of sensors on connected segments'. Assuming that adjacent segments are connected and that an IMU is placed on each segment, it has been shown that under mild

conditions on the motion of the body segments [14], drift-free estimates of the relative orientation can be obtained by exploiting common information in the inertial sensor measurements [15], [16]. In [16], an optimisation-based smoothing approach was presented to exploit this information, while [15] presented both a filtering and a smoothing approach.

Although existing methods allow for the estimation of accurate relative sensor orientation estimates, optimization-based smoothing approaches inherently result in high computational complexity. Furthermore, real-life disturbances that commonly occur during joint kinematic estimation can cause the estimation algorithm's accuracy to rapidly decrease if they violate the model assumptions [17]. Such disturbances naturally arise when sensors are placed on human body segments due to STA. In addition, accelerometer outliers caused by impacts on external surfaces of the sensor or the body that the sensor is placed, need to be compensated for.

In this paper, we present a novel complementary filtering approach using similar models as in [15] for the estimation of relative sensor orientations. We show that our algorithm is computationally more efficient than the filtering algorithm presented in [15]. Our algorithm takes inspiration from the complementary filter presented in [18] to estimate the absolute sensor orientation of a single IMU. That algorithm was shown to be robust against outliers in the accelerometer measurements. We study the robustness against accelerometer outliers and STA of our algorithm, and show that it is robust against outliers and to a certain degree also against STA.

In Section II we present the different sensor models and the kinematic model. Section III presents our algorithm. Section IV studies the robustness of our algorithm against model violations with numerical simulations. Finally, a human experiment strengthens the simulation results and conclusions in Section V. The final conclusion and extensions for future works are given in Section VI.

II. Modeling

We are interested in estimating the relative sensor orientation of IMUs which are placed on adjacent human body segments. We assume that these segments are rigid and connected via a spherical joint [15]. Without loss of generality we focus our discussion on only two body segments and their connected sensors, with corresponding sensor coordinate frames S_i, $i = 1, 2$. These coordinate frames are aligned with the inertial sensor axes and their origin is located at the center of the i'th accelerometer triad. We estimate the orientation at time step t of both sensors in terms of unit quaternions $q_t^{\mathrm{GS}_i}$, representing the orientations at time instance t from the frames S_i, $i = 1, 2$ to the frame G. The frame G is a fixed geographic frame that is aligned with the gravity vector. The alignment of the frame G can without loss of generality arbitrarily be chosen since our interest does not lie in the absolute orientations $q_t^{\mathrm{GS}_i}$ but in the relative orientations $q_t^{\mathrm{S}_1\mathrm{S}_2}$, which can be computed from the estimates $q_t^{\mathrm{GS}_i}$ but do not depend on the specific choice of the alignment of the frame G.

A. Sensor models

We model the measurements of the gyroscope $y_{\omega,t}^{\mathrm{S}_i}$ as

$$y_{\omega,t}^{\mathrm{S}_i} = \omega_t^{\mathrm{S}_i} + e_{\omega,t}^{\mathrm{S}_i}, \tag{1}$$

where $\omega_t^{\mathrm{S}_i}$ denotes the angular velocity and $e_{\omega,t}^{\mathrm{S}_i}$ the measurement noise at time step t. The superscripts explicitly indicate that these quantities are expressed in the sensor frame S_i.

We assume that the accelerometer measures the Earth's gravity g^{G} accompanied by a linear acceleration a^{G}. The accelerometer measurements $y_{\mathrm{a},t}^{\mathrm{S}_i}$ are therefore modeled as

$$y_{\mathrm{a},t}^{\mathrm{S}_i} = R\left(q_t^{\mathrm{S}_i\mathrm{G}}\right)\left(a_t^{\mathrm{G}} - g^{\mathrm{G}}\right) + e_{\mathrm{a},t}^{\mathrm{S}_i}, \tag{2}$$

where $e_{\mathrm{a},t}^{\mathrm{S}_i}$ denotes the measurement noise of i'th accelerometer. The operation $R(q_t^{\mathrm{GS}_i})$ converts the unit quaternion $q_t^{\mathrm{GS}_i}$ to a rotation matrix [7] and $R(q_t^{\mathrm{GS}_i}) = (R(q_t^{\mathrm{S}_i\mathrm{G}}))^\top$.

B. Joint Kinematic Modeling

As illustrated in Fig. 1, we consider the case of two adjacent body segments that connect at a common point, the joint center jc. It is possible to compute the acceleration at this common point expressed in the two rigidly attached inertial sensor frames as in [15]

$$\begin{aligned} a_{\mathrm{jc},t}^{\mathrm{S}_i} &= y_{a,t}^{\mathrm{S}_i} - \mathcal{C}_t^{\mathrm{S}_i} r_i^{\mathrm{S}_i}, \\ \mathcal{C}_t^{\mathrm{S}_i} &= \left[y_{\omega,t}^{\mathrm{S}_i}\times\right]^2 + \left[\dot{y}_{\omega,t}^{\mathrm{S}_i}\times\right]. \end{aligned} \tag{3}$$

Here, $[\,\cdot\,\times]$ denotes the cross-product matrix and $\dot{y}_{\omega,t}^{\mathrm{S}_i}$ the angular acceleration of the i'th sensor at time instance t. Furthermore, the vectors $r_1^{\mathrm{S}_1}$ and $r_2^{\mathrm{S}_2}$ denote the distance from the IMU to the joint center [19], [20].

The difference in the joint center accelerations $a_{\mathrm{jc},t}^{\mathrm{S}_1}$ and $a_{\mathrm{jc},t}^{\mathrm{S}_2}$ computed from the measurements of the two inertial sensors should be zero (up to inertial measurement errors), when expressed in a common global frame G. Hence,

$$R_t^{\mathrm{GS}_1} a_{\mathrm{jc},t}^{\mathrm{S}_1} = R_t^{\mathrm{GS}_2} a_{\mathrm{jc},t}^{\mathrm{S}_2} + e_{\mathrm{link},t}, \tag{4}$$

where $e_{\mathrm{link},t}$ denotes the error due to measurement noise of the accelerometers and gyroscopes or disturbances. We will use the model (4) in our complementary filtering approach in Section III to provide information about the relative orientation between the two sensors.

III. Methods

To estimate the relative sensor orientation of two inertial sensors placed on connected body segments, we jointly estimate the orientations $q_t^{\mathrm{GS}_1}$ and $q_t^{\mathrm{GS}_2}$. In Section III-A we outline our general approach, summarized in Algorithm 1. We use a complementary filtering approach to compute the orientations using the gyroscope measurements modeled as in (1) and correct these estimates using the joint kinematic model (4) in Section III-B.

A. Estimating the relative sensor orientation

We jointly estimate the orientations $\hat{q}_t^{\mathrm{GS}_i}$ of the sensors S_i, $i = 1, 2$ using a complementary filtering approach. Following [18], we interpret our estimation problem in terms of estimating angular velocities $\hat{\omega}_t^{\mathrm{S}_i}$, $i = 1, 2$. These are subsequently used to update the orientation estimate $\hat{q}_{t-1}^{\mathrm{GS}_i}$ as [7], [21].

$$\hat{q}_t^{\mathrm{GS}_i} = \hat{q}_{t-1}^{\mathrm{GS}_i} \odot \exp_{\mathrm{q}}\left(\frac{T}{2}\hat{\omega}_t^{\mathrm{S}_i}\right), \tag{5a}$$

$$\approx \hat{q}_{t-1}^{\mathrm{GS}_i} + \frac{T}{2} S\left(\hat{q}_{t-1}^{\mathrm{GS}_i}\right)\hat{\omega}_t^{\mathrm{S}_i}, \qquad i = 1, 2, \tag{5b}$$

where T denotes the sampling time, $\odot$ the quaternion product and

$$\begin{aligned} \exp_{\mathrm{q}}(\omega) &= \begin{pmatrix} \cos\alpha & v^\top \sin\alpha \end{pmatrix}^\top, \\ \alpha &= \|\omega\|_2, \quad v = \frac{\omega}{\alpha}, \end{aligned} \tag{6}$$

with $\|\cdot\|_2$ denoting the two-norm. Furthermore,

$$S(q) = \begin{pmatrix} -q_v \\ q_0\mathcal{I}_3 - [q_v\times] \end{pmatrix}, \tag{7}$$

for $q = \begin{bmatrix} q_0 & q_1 & q_2 & q_3 \end{bmatrix}^\top = \begin{bmatrix} q_0 & q_v^\top \end{bmatrix}^\top$. Note that we use the approximation (5b) to reduce computational complexity.

We estimate the angular velocities from the gyroscope measurements $y_{\omega,t}^{\mathrm{S}_i}$, $i = 1, 2$ and a correction based on the model (4) as

$$\hat{\omega}_t^{\mathrm{S}_i} = y_{\omega,t}^{\mathrm{S}_i} - \Delta\hat{\omega}_{\mathrm{link},i,t}^{\mathrm{S}_i}, \qquad i = 1, 2. \tag{8}$$

The computation of the correction $\Delta\hat{\omega}_{\mathrm{link},i,t}^{\mathrm{S}_i}$ will be detailed in Section III-B.

The relative orientation between the sensors can subsequently be computed as

$$\hat{q}_t^{\mathrm{S}_1\mathrm{S}_2} = \left(\hat{q}_t^{\mathrm{GS}_1}\right)^c \odot \hat{q}_t^{\mathrm{GS}_2}, \tag{9}$$

where the superscript c denotes the quaternion conjugate [7]. The resulting algorithm is presented in Algorithm 1.

Note that an alternative interpretation of (5b) and (8) is that in Algorithm 1 we first update the orientation with the gyroscope measurements (similar to a filtering time update) and subsequently correct the estimate using information from the joint kinematic model (similar to a measurement update). However, first computing an estimate of the angular velocity and then using that estimate to update the orientation was shown in [18] to be computationally more efficient, while in other respects being similar to the widely used approach from [22], [23]. Note also that the crucial difference between Algorithm 1 and the one presented in [18] is that we consider the case of jointly estimating the orientation of multiple IMUs placed on connected segments, rather than estimating the orientation of a single IMU. This enables us to exploit the joint kinematic model (4).

Algorithm 1 Relative sensor orientation estimation

Input: Gyroscope and accelerometer measurements $y_{\omega,t}^{\mathrm{S}_i}$, $y_{\mathrm{a},t}^{\mathrm{S}_i}$, the orientation estimate at the previous time instance $\hat{q}_{t-1}^{\mathrm{GS}_i}$, the distances from the IMUs to the joint center $r_1^{\mathrm{S}_1}$, $r_2^{\mathrm{S}_2}$, the tuning parameter β and the sampling time T.

Output: Relative sensor orientation estimate $\hat{q}_t^{\mathrm{S}_1\mathrm{S}_2}$.

1: Compute the gradient (13) at time instance t using $\hat{q}_{t-1}^{\mathrm{GS}_i}$ and $a_{\mathrm{jc},t}^{\mathrm{S}_i}$ determined according to (3).
2: Compute the estimated angular velocities $\hat{\omega}_t^{\mathrm{S}_i}$, $i = 1, 2$ according to (8) and (12).
3: Compute the orientation estimates $\hat{q}_t^{\mathrm{GS}_i}$, $i = 1, 2$ according to (5b) using $\hat{\omega}_t^{\mathrm{S}_i}$ and $\hat{q}_{t-1}^{\mathrm{GS}_i}$.
4: Compute the relative sensor orientation $\hat{q}_t^{\mathrm{S}_1\mathrm{S}_2}$ from $\hat{q}_t^{\mathrm{GS}_i}$, $i = 1, 2$ according to (9).

B. Computing the correction to the angular velocity

We formulate estimation of the orientation of both sensors using the model (4) as an optimization problem as

$$\begin{aligned} \min_{\eta_t} V(\eta_t) = \min_{\eta_t} \frac{1}{2} \Big\| & R\left(\tilde{q}_t^{\mathrm{GS}_1}\right)\left(\mathcal{I}_3 + [\eta_{\mathrm{S}_1,t}\times]\right) a_{\mathrm{jc},t}^{\mathrm{S}_1} \\ & - R\left(\tilde{q}_t^{\mathrm{GS}_2}\right)\left(\mathcal{I}_3 + [\eta_{\mathrm{S}_2,t}\times]\right) a_{\mathrm{jc},t}^{\mathrm{S}_2} \Big\|_2^2, \end{aligned} \tag{10}$$

where $\eta_t = \begin{bmatrix} \eta_{\mathrm{S}_1,t}^\top & \eta_{\mathrm{S}_2,t}^\top \end{bmatrix}^\top$. Inspired by [7], [18], in (10) we write the orientation in terms of linearization points $\tilde{q}_t^{\mathrm{GS}_1}$, $\tilde{q}_t^{\mathrm{GS}_2}$ and associated deviations $\eta_{\mathrm{S}_1,t}$, $\eta_{\mathrm{S}_2,t}$ as

$$R\left(q_t^{\mathrm{GS}_i}\right) = R\left(\tilde{q}_t^{\mathrm{GS}_i}\right)\exp_{\mathrm{R}}\left(\eta_{\mathrm{S}_i,t}\right), \tag{11a}$$

$$\begin{aligned} \exp_{\mathrm{R}}\left(\eta_{\mathrm{S}_i,t}\right) &= \mathcal{I}_3 + \sin\alpha[v\times] + (1-\cos\alpha)[v\times]^2 \\ &\approx \mathcal{I}_3 + [\eta_{\mathrm{S}_i,t}\times], \end{aligned} \tag{11b}$$

with $\alpha = \|\eta_{\mathrm{S}_i,t}\|_2$ and $v = \frac{\eta_{\mathrm{S}_i,t}}{\alpha}$. The approximation in (11b) is valid for small $\eta_{\mathrm{S}_i,t}$ [7]. By rewriting the problem in this fashion, we optimize over orientation deviations parametrized as rotation vectors, avoiding the inclusion of constraints that would be necessary for other orientation parametrizations and reducing the size of the optimization variable to $\mathbb{R}^6$.

Like [18], [22], [23], at each time step we only perform a single gradient descent iteration of (10). This decreases the computational time and because of the high sampling frequency of the sensors, the corrections that need to be made are typically minor and the estimates will converge over time. Furthermore, we choose to normalize the gradient step at each iteration, which has been shown to result in robustness against model inaccuracies in previous work [18] for the case of orientation estimation using a single IMU. Hence, we compute the correction to the angular velocity estimate from the model (4) as

$$\begin{pmatrix} \Delta\hat{\omega}_{\mathrm{link},1,t}^{\mathrm{S}_1} \\ \Delta\hat{\omega}_{\mathrm{link},2,t}^{\mathrm{S}_2} \end{pmatrix} = \beta\frac{\nabla V(\eta_t)}{\|\nabla V(\eta_t)\|_2}, \tag{12}$$

where β is a tuning parameter which can be chosen based on the amount of drift expected from the gyroscope integration [18], [22]. Here, $\nabla V(\eta_t)$ denotes the gradient of (10), linearized around $\tilde{q}_t^{\mathrm{GS}_i} = \hat{q}_{t-1}^{\mathrm{GS}_i}$ and $\eta_t = 0_{6\times 1}$, given by

$$\begin{aligned}\nabla V(\eta_t) = \Bigg(&-R\left(\hat{q}_{t-1}^{\mathrm{GS}_1}\right)\begin{bmatrix}\left[a_{\mathrm{jc},t}^{\mathrm{S}_1}\times\right] & 0_{3\times 3}\end{bmatrix}\\ &+R\left(\hat{q}_{t-1}^{\mathrm{GS}_2}\right)\begin{bmatrix}0_{3\times 3} & \left[a_{\mathrm{jc},t}^{\mathrm{S}_2}\times\right]\end{bmatrix}\Bigg)^{\top}\\ &\left(R\left(\hat{q}_{t-1}^{\mathrm{GS}_1}\right)a_{\mathrm{jc},t}^{\mathrm{S}_1} - R\left(\hat{q}_{t-1}^{\mathrm{GS}_2}\right)a_{\mathrm{jc},t}^{\mathrm{S}_2}\right).\end{aligned} \tag{13}$$

IV. Numerical simulation

To study the performance of Algorithm 1 in the presence of real-life disturbances and to demonstrate its computational benefits, we run 100 Monte Carlo simulations for different noise realizations and simulated disturbances. We compare the results from Algorithm 1 with those from the multiplicative extended Kalman filter (MEKF) presented in [15] and a slightly adapted MEKF that includes outlier rejection [21]. The MEKFs use the same models as those used in Algorithm 1. A minor difference is that they use the exact filtering time update (5a) instead of the approximation (5b). The evaluation is done by calculating the average angular distance $\bar{\theta}$ between the ground-truth and the estimated orientation, $\hat{q}_t^{\mathrm{S}_1\mathrm{S}_2}$ [24] and its standard deviation $\sigma_{\bar{\theta}}$.

Each simulation consists of 800 seconds of data with a sampling rate of 10 Hz. The simulated movement represents two IMUs on connected segments, that rotate in opposite directions with an angular velocity $y_{\omega,t}^{\mathrm{S}_i}$ that is modeled as $\pm\sin\left(\frac{\pi}{100T}t\right)$ and sequentially applied onto the three orthogonal sensor axes. Accelerometer measurements $y_{a,t}^{\mathrm{S}_i}$ were constructed following (3) with the joint center acceleration $a_{\mathrm{jc},t}^{\mathrm{G}}$ randomly sampled from a uniform distribution taking values in the range -10 to 10 $\mathrm{m/s^2}$, and subsequently rotated to S_1 and S_2. The distances of the sensors to the joint center were set to $r_1^{\mathrm{S}_1} = [1 \quad 0 \quad 0]^{\top}$, $r_2^{\mathrm{S}_2} = [-1 \quad 0 \quad 0]^{\top}$. Measurement noise was added to the data with $e_{\omega,t} \sim \mathcal{N}\left(0, \sigma_\omega^2 \mathcal{I}_3\right)$, $e_{a,t} \sim \mathcal{N}\left(0, \sigma_{\mathrm{a}}^2 \mathcal{I}_3\right)$ where $\sigma_\omega = \frac{\pi}{180}$ rad/s, $\sigma_a = \frac{9.81}{100}$ $\mathrm{m/s^2}$. Note that these values are significantly larger than is typically the case for IMUs, to more clearly demonstrate the properties of the filters. Angular accelerations $\dot{y}_{\omega,t}^{\mathrm{S}_i}$ were approximated from the simulated gyroscope measurements with a five-point stencil [25].

The simulations were processed in Matlab (R2020a, Mathworks, USA) on a laptop (Intel Core i5 7th generation) for both Algorithm 1 and the MEKF presented in [15], with and without outlier rejection. The initial orientations $\hat{q}_1^{\mathrm{GS}_i}$, $i = 1, 2$ were set to $[1 \quad 0 \quad 0 \quad 0]^{\top}$ for the three filtering algorithms.

In line with [18], we set β in Algorithm 1 equal to $\sqrt{3}\sigma_\omega$. Note that lowering the value of β in (12), (8) entails relying more on the orientation obtained by gyroscope integration, while increasing the value of β entails relying more on the orientation obtained by the joint kinematic constraint. The process and measurement noise covariances in the MEKF from [15] were chosen based on σ_{a}, σ_ω and assuming that the accelerometer measurement noise is the dominant source of error in (4).

We first study the performance of the different filters in the absence of disturbances. As can be seen in Table I, in this case the MEKF without outlier rejection slightly outperforms Algorithm 1. This is in line with the results from [18], the fact that extended Kalman filters are known to perform well for orientation estimation using inertial sensors [7] and the fact that Algorithm 1 only performs one normalized gradient descent step (13) to optimize (10) at each time instance. The latter is also the reason why the computational complexity of Algorithm 1 can be seen to be significantly lower than that of the MEKF from [15]. The reason for the MEKF to slightly outperform the MEKF with outlier rejection could be that some measurements are wrongfully considered to be outliers. In Sections IV-A and IV-B we will study the effect of outliers and STA on the estimates from the different algorithms.

	$\theta \pm \sigma_{\bar{\theta}}$ [°]			Time per iteration [μs]		
	Alg. 1	MEKF [15]	MEKF with o.r. [15]	Alg. 1	MEKF [15]	MEKF with o.r. [15]
No dist.	0.71± 0.008	**0.59**± **0.007**	0.62± 0.008	**4.16**	94.8	102
5% acc. outliers	0.75± 0.010	3.11± 0.109	**0.65**± **0.040**	**4.16**	94.8	102
Lowest STA	0.71± 0.008	**0.59**± **0.007**	0.64± 0.081	**4.16**	94.8	102
Middle STA	0.82± 0.011	**0.73**± **0.009**	0.89± 0.084	**4.16**	94.8	102
Highest STA	**1.52**± **0.056**	3.62± 0.059	1.99± 0.260	**4.16**	94.8	102

TABLE I: Average angular distance $\bar{\theta}$ and its standard deviation $\sigma_{\bar{\theta}}$ in the relative sensor orientation and computational times for the five Monte Carlo analyses and the three algorithms (outlier rejection abbreviated as o.r.).

A. Accelerometer model inaccuracies

Outliers in the accelerometer measurements can occur in practice due to impacts on external surfaces of the sensor or the body it is mounted on. We simulate such accelerometer outliers for 5% of the simulated accelerometer data starting after 100 seconds, which is used as a settling time for the filters. This relatively large percentage of accelerometer outliers is used to illustrate the effect of outliers on the estimates of the filters. The outliers are created from a uniform distribution, with a random direction and a magnitude between 50 and 100 times the standard deviation of the accelerometer. As shown in Table I, these outliers greatly influence the estimation performance of the MEKF while the orientation errors remain small for Algorithm 1 and the MEKF with outlier rejection.

B. Soft Tissue Artifacts

Since it is not possible to place sensors directly on the bone, disturbances caused by the non-rigidity of the tissue, so called STA, are unavoidable. Such disturbances naturally violate the assumption in (3) on the sensor locations $r_i^{\mathrm{S}_i}$ being constant. This typically leads to disturbances in the

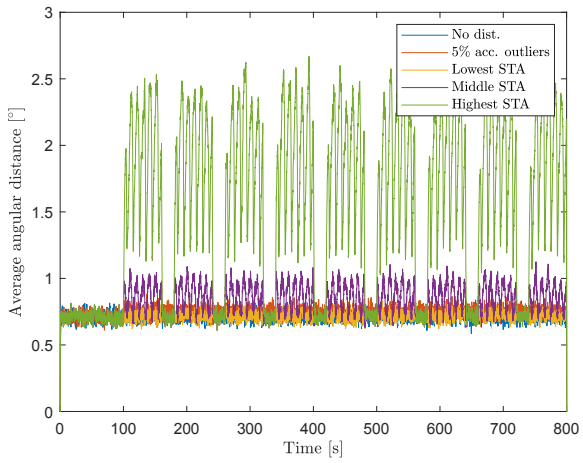

Fig. 2: Average angular distance from Algorithm 1 for the five different numerical simulations.

acceleration measurements [20]. Following [20], [26], we model these acceleration disturbances $d_{\text{STA},t}^{\text{S}_i}$ as

$$d_{\text{STA},t}^{\text{S}_i} = H_t^{\text{S}_i} \dot{\omega}_t^{\text{S}_i}. \tag{14}$$

The matrix $H_t^{\text{S}_i} \in \mathbb{R}^{3\times 3}$ contains the parameters to model the STA for the i'th sensor at time step t. Again, we model the STA after 100 seconds to allow for settling of the filters.

In practice, the elements of $H_t^{\text{S}_i}$ depend on multiple factors, e.g., sensor placement and the subject's physiology [20]. We simulated three different levels of STA. Following [20], we created the lowest levels of STA and continue to increase the levels of STA to study the robustness properties of Algorithm 1. To this end, $H_t^{\text{S}_i}$ was filled with samples from a normal distribution with zero mean and standard deviation σ_{STA}. The lowest levels of STA were created by setting $\sigma_{\text{STA}} = \frac{0.018}{\pi}$ m/rad. This resulted in a maximal disturbance value of $8.7 \cdot 10^{-3}$ m/s^2, which translates to a displacement of 87 μm after 10^{-1} seconds. The mid-levels of STA were created with $\sigma_{\text{STA}} = \frac{1.8}{\pi}$ m/rad, which lead to a maximum displacement of 0.87 cm. The highest levels of simulated STA were created by setting $\sigma_{\text{STA}} = \frac{18}{\pi}$ m/rad, leading to a maximum displacement of 8.68 cm.

Both the MEKF from [15] (with and without outlier rejection) and Algorithm 1 are able to cope with the disturbances induced by the lowest and mid-levels of simulated STA as can been seen from Table I. However, in contrast to the MEKF from [15], Algorithm 1 and the MEKF with outlier rejection also show robustness to a lesser extent against the highest level of STA. In Fig. 2, the average angular distance from Algorithm 1 over time is shown for the different simulations. During the moments where STA occurs, the assumed model violations increase which can be seen to result in an increase in the errors.

V. Experimental Results

We also study the robustness against disturbances of Algorithm 1 for a real-world movement analysis application. One healthy subject gave his written informed consent to perform a stand-still phase of five seconds and three functional movement trials consisting of two gait trials and one set of forward lunge movements [27].

Inertial sensors (MTw Awinda IMU from Xsens) were attached on the lateral side at mid-distance on the shank and on the thigh via Velcro strips as shown in Fig. 3. The sensor placement was altered for the second and third functional movement to a more anterior position, resulting in an assumed higher level of STA. An optical motion capture system (13 camera VICON Vero, Vicon Motion Systems Ltd) served as reference by tracking infrared reflective marker clusters attached to the IMUs housing. A hardware time synchronization was used to simultaneously capture inertial measurements and optical marker trajectories at a sample frequency of 100 Hz. The study has been approved by the medical-ethical committee of UZ Leuven (Nr. S58936) and adhered to the declaration of Helsinki.

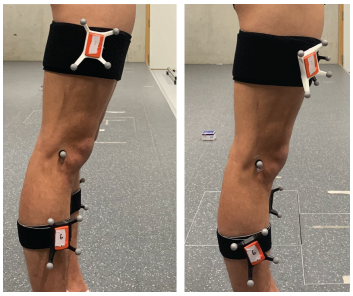

Fig. 3: Experimental set-up with inertial sensors attached on the thigh and shank segments for a lateral placement (left) and more anterior placement (right).

We applied both Algorithm 1 and the MEKF from [15] (with and without outlier rejection), to the experimental data to obtain relative orientation estimates for the knee joint. To compare the orientation estimates to those from the optical motion capture system, constant misalignments between the inertial sensor sensing axes and coordinate systems on the base of three optical markers were acquired from relative orientations measurements and estimated following [15]. The orientation estimates were evaluated during motion, ignoring the static time period at the start of each experiment. All three algorithms were tuned to result in the lowest angular distance with respect to the reference data. The values for $r_1^{\text{S}_1}$ and $r_2^{\text{S}_2}$ were estimated following [20], by minimizing the sum of absolute errors to gain robustness against outliers. The initial orientations $\hat{q}_1^{\text{GS}_i}$, $i = 1, 2$ were set to $\begin{bmatrix}1 & 0 & 0 & 0\end{bmatrix}^\top$ for the three filtering algorithms.

In Table II we observe that the MEKF from [15] and Algorithm 1 perform similarly for a first gait trial with lateral sensor placement, but the MEKF with outlier rejection outperforms both methods by rejecting accelerometer measurements which are corrupted by STA. Adapting the sensor placement to a more anterior position, we expect more STA and hence an increase in the violations of the model (3) and a decrease in the accuracy of the orientation estimates. The forward lunge motion is expected to present even higher

levels of STA during initial contact, where the heel touches the ground [27]. This resulted in larger estimation errors for all algorithms. The lower performance of Algorithm 1 during the lunge trials seems related to large initialization errors. For the case of large STA resulting in violations of the model (3) one would prefer to choose a very small value for β, which entails relying more on the gyroscope. However, this also entails a slow convergence rate. Our empirically optimized value for β for this experiment was equal to the relatively large value of 1, resulting in a relatively large sensitivity to outliers but a fast convergence.

	Angular distance θ [°]		
	Alg. 1	MEKF [15]	MEKF with o.r. [15]
Gait (lateral)	1.85	1.48	**0.94**
Gait (anterior)	2.19	1.79	**1.74**
Lunge (anterior)	8.40	3.87	**3.69**

TABLE II: Angular distance θ in the relative orientation for the three experiments and the three algorithms (outlier rejection abbreviated as o.r.).

VI. Conclusions and future work

We have presented an algorithm to estimate the relative sensor orientation between two sensors placed on adjacent body segments. The algorithm is computationally efficient, opening up for the processing of large data sets to analyze human motion. The algorithm has been shown in simulations and in experiments to be robust to outliers in the accelerometer data and to a certain degree to model inaccuracies due to STA. The accuracy of the estimates for larger STA, however, still degrades and this is an interesting topic for future work. It would, for instance, be interesting to investigate a dynamic rather than static value for β, to ensure both convergence and robustness. Additionally, future work could extend the measurement models, for instance including sensor biases. Another topic for future work could be on the validation of experiments where a range of multiple and highly dynamic movements are performed.

Acknowledgement

The conducted human experiments were funded by the European Regional Development Fund – We-lab for HTM [grant number 1047].

References

[1] I. H. López-Nava and A. Muñoz-Meléndez, "Wearable inertial sensors for human motion analysis: A review," *IEEE Sensors Journal*, vol. 16, no. 22, pp. 7821–7834, 2016.

[2] P. Picerno, "25 years of lower limb joint kinematics by using inertial and magnetic sensors: A review of methodological approaches," *Gait & Posture*, vol. 51, pp. 239 – 246, 2017.

[3] M. Noorkõiv, H. Rodgers, and C. I. Price, "Accelerometer measurement of upper extremity movement after stroke: a systematic review of clinical studies," *Journal of neuroengineering and rehabilitation*, vol. 11, no. 144, 2014.

[4] S. G. Trost, K. L. Mciver, and R. R. Pate, "Conducting accelerometer-based activity assessments in field-based research," *Medicine & science in sports & exercise*, vol. 37, no. 11, pp. S531–S543, 2005.

[5] V. Camomilla, A. Cappozzo, and G. Vannozzi, *Three-Dimensional Reconstruction of the Human Skeleton in Motion*. Cham: Springer International Publishing, 2017, pp. 1–29.

[6] A. Chadwell, L. Kenney, M. Granat, S. Thies, J. S. Head, and A. Galpin, "Visualisation of upper limb activity using spirals: A new approach to the assessment of daily prosthesis usage," *Prosthetics and orthotics international*, vol. 42, no. 1, pp. 37–44, 2018.

[7] M. Kok, J. D. Hol, and T. B. Schön, "Using inertial sensors for position and orientation estimation," *Foundations and Trends in Signal Processing*, vol. 11, no. 1-2, pp. 1–153, 2017.

[8] W. de Vries, H. Veeger, C. Baten, and F. van der Helm, "Magnetic distortion in motion labs, implications for validating inertial magnetic sensors," *Gait & Posture*, vol. 29, no. 4, pp. 535 – 541, 2009.

[9] E. R. Bachmann, X. Yun, and C. W. Peterson, "An investigation of the effects of magnetic variations on inertial/magnetic orientation sensors," in *Proceedings of the IEEE International Conference on Robotics and Automation (ICRA)*, New Orleans, LA, USA, Apr.–May 2004.

[10] D. Laidig, D. Lehmann, M. Bégin, and T. Seel, "Magnetometer-free realtime inertial motion tracking by exploitation of kinematic constraints in 2-DoF joints," in *Proceedings of the 41st Annual International Conference of the IEEE Engineering in Medicine and Biology Society (EMBC)*, Berlin, Germany, July 2019.

[11] D. Laidig, T. Schauer, and T. Seel, "Exploiting kinematic constraints to compensate magnetic disturbances when calculating joint angles of approximate hinge joints from orientation estimates of inertial sensors," in *Proceedings of the International Conference on Rehabilitation Robotics (ICORR)*, London, UK, July 2017.

[12] T. Seel, J. Raisch, and T. Schauer, "IMU-based joint angle measurement for gait analysis," *Sensors*, vol. 14, no. 4, pp. 6891–6909, 2014.

[13] D. L. Benoit, D. K. Ramsey, M. Lamontagne, L. Xu, P. Wretenberg, and P. Renström, "In vivo knee kinematics during gait reveals new rotation profiles and smaller translations." *Clinical Orthopaedics and Related Research*, vol. 454, pp. 81–88, 2007.

[14] M. Kok, K. Eckhoff, I. Weygers, and T. Seel, "Observability of the relative motion from inertial data in kinematic chains," *ArXiv e-prints*, 2021, arXiv:2102.02675.

[15] I. Weygers, M. Kok, H. De Vroey, T. Verbeerst, M. Versteyhe, H. Hallez, and K. Claeys, "Drift-Free Inertial Sensor-Based Joint Kinematics for Long-Term Arbitrary Movements," *IEEE Sensors Journal*, vol. 20, no. 14, pp. 7969–7979, 2020.

[16] M. Kok, J. D. Hol, and T. B. Schön, "An optimization-based approach to human body motion capture using inertial sensors," *IFAC Proceedings Volumes*, vol. 47, no. 3, pp. 79–85, 2014.

[17] W. Teufl, M. Miezal, B. Taetz, M. Fröhlich, and G. Bleser, "Validity, test-retest reliability and long-term stability of magnetometer free inertial sensor based 3D joint kinematics," *Sensors*, vol. 18, no. 7, p. 1980, 2018.

[18] M. Kok and T. B. Schön, "A Fast and Robust Algorithm for Orientation Estimation using Inertial Sensors," *IEEE Signal Processing Letters*, vol. 26, no. 11, pp. 1673–1677, 2019.

[19] T. Seel, T. Schauer, and J. Raisch, "Joint axis and position estimation from inertial measurement data by exploiting kinematic constraints," in *Proceedings of the IEEE International Conference on Control Applications*, Dubrovnik, Croatia, Oct. 2012.

[20] F. Olsson and K. Halvorsen, "Experimental evaluation of joint position estimation using inertial sensors," in *Proceedings of the 20th International Conference on Information Fusion*, Xi'an, China, July 2017, pp. 1–8.

[21] F. Gustafsson, *Statistical Sensor Fusion*. Studentlitteratur, 2012.

[22] S. Madgwick, "An efficient orientation filter for inertial and inertial/magnetic sensor arrays," *Report x-io and University of Bristol (UK)*, vol. 25, pp. 113–118, 2010.

[23] S. O. Madgwick, A. J. Harrison, and R. Vaidyanathan, "Estimation of IMU and MARG orientation using a gradient descent algorithm," in *Proceedings of the IEEE international conference on rehabilitation robotics*, Zurich, Switzerland, Jun–Jul. 2011.

[24] R. Hartley, J. Trumpf, Y. Dai, and H. Li, "Rotation averaging," *International journal of computer vision*, vol. 103, no. 3, pp. 267–305, 2013.

[25] T. Sauer, *Numerical Analysis*. Pearson, 2012, vol. 2.

[26] V. Camomilla, A. Cereatti, L. Chèze, and A. Cappozzo, "A hip joint kinematics driven model for the generation of realistic thigh soft tissue artefacts," *Journal of biomechanics*, vol. 46, no. 3, pp. 625–630, 2013.

[27] H. De Vroey, F. Staes, I. Weygers, E. Vereecke, G. Van Damme, H. Hallez, and K. Claeys, "Hip and knee kinematics of the forward lunge one year after unicondylar and total knee arthroplasty," *Journal of Electromyography and Kinesiology*, vol. 48, pp. 24–30, 2019.